Taylor & Francis
Taylor & Francis Group

Automatika
Journal for Control, Measurement, Electronics, Computing and Communications

ISSN: (Print) (Online) Journal homepage: www.tandfonline.com/journals/taut20

Seven levels highly efficient modular multilevel matrix converter (M3C) for low frequency three-phase AC-AC conversion

V. Karpagam & N. Narmadhai

To cite this article: V. Karpagam & N. Narmadhai (2023) Seven levels highly efficient modular multilevel matrix converter (M3C) for low frequency three-phase AC-AC conversion, Automatika, 64:4, 1255-1267, DOI: 10.1080/00051144.2023.2253067

To link to this article: https://doi.org/10.1080/00051144.2023.2253067

AUTOMATIKA
2023, VOL. 64, NO. 4, 1255–1267
https://doi.org/10.1080/00051144.2023.2253067

Taylor & Francis
Taylor & Francis Group

Seven levels highly efficient modular multilevel matrix converter (M3C) for low frequency three-phase AC-AC conversion

V. Karpagam[a] and N. Narmadhai[b]

[a]Dr. Mahalingam College of Engineering and Technology, Pollachi, India; [b]Department of EEE, Government College of Technology, Coimbatore, India

ABSTRACT
An Innovative Modular multilevel matrix converter (M3C) is proposed with reduced number of switching device owing to the improved efficiency, reduced cost and minimizes the size. Offshore Low-Frequency AC (LFAC) transmissions are economical with greater reliability for short and intermediate distance transmissions. Similar to HVDC, it increases the transmission capacity and also distance can be increased in LFAC.M3C is proposed as frequency converters for LFAC transmissions which link AC systems operating at 16.7 and 50 Hz. The double $\alpha\beta 0$ transform control technique has been the most often used approach for decoupling control of input, output and circulating currents in such applications. The performances of this work's proposed modular multilevel matrix converters are analysed using simulation in MATLAB/SIMULINK software.

ARTICLE HISTORY
Received 12 May 2023
Accepted 23 August 2023

KEYWORDS
Modular multilevel matrix converter (M3C); PMSG wind turbine; MOSFET; power grid; offshore low frequency AC (LFAC) transmission; branch energy balance circuit

1. Introduction

Energy depletions, global warming and environmental deteriorations have become the greatest threats to sustainable development of human societies. Hence, globally, governments are prioritizing green and low-carbon frameworks which are based on renewable energies and reduced emissions. Typically, geographical constraints and the rapid expansion of wind farm capacity necessitate the placement of wind farms. The main electrical grid or significant load centres are often far remote from a wind farm [1,2]. The transfer of wind energy from an offshore wind farm in a remote area has been raised as an essential issue in light of these instances. The primary objective is to determine how to increase transmission distance and capacity. LFAC (16.7 Hz) transmission systems are considered good future choices in constructions of offshore wind farms, in addition to conventional High system (HVAC) and High voltage DC (HVDC) transmission systems, Low frequency alternating current (LFAC) transmissions have two main advantages over HVDC transmissions namely lower costs and greater efficiencies: (1) increased transmission capacity and greater transmission range due to lower charging current due to the low frequency; and (2) lower construction and maintenance costs due to the use of a single onshore AC/AC converter [3–5].

Onshore AC/AC converters are the most essential components in LFAC transmissions. The cycloconverter is the most frequently used frequency converter. However, its continued improvements are constrained by strong harmonics and low power factors [6]. M3C has been recognized as next generation AC/AC converters due to their high levels of flexibility/scalability, excellent power qualities and adaptability to accommodate power factors of both sides. However, the control of the M3C poses challenges for its application to the LFAC transmission system. Recently, academic scholars have been interested in the promising and growing technology known as LFAC. When comparing to a 50 Hz system, it delivers up to three times the transmission capacity, which significantly lowers the investment costs [7,8].

A number of conventional and derived topologies have been presented in the literature, with power electronic converters serving as the primary enablers for the establishment of LFAC. For instance, a cycloconverter for the LFAC system is developed and experimentally tested, although there are downsides and restrictions that were discovered. This also refers to the need for reactive power adjustment and the inability to ride through faults. Modern back-to-back Modular Multilevel Converters (MMC) is also viable alternatives due to their distinct qualities which includes modularity, scalability to meet multiple voltage level requirements and superior harmonic performances [9–14].

But the dc-link's results in increased power losses and decreased system dependability. The M3C idea and operation were initially described in [15], and its control strategy was later detailed in [16]. Two-level switching is used to provide space vector control and the study demonstrates that M3C can circumvent the typical matrix converters' gain restriction of 0.866. Nine converter arms serves as current sources in new M3C structures with arm inductors that were

CONTACT V. Karpagam karpagam.vellingiri@gmail.com Dr. Mahalingam College of Engineering and Technology, Pollachi, India

subsequently developed in [17] could independently control input and output currents. However, the use of a six times transformation matrix in its energy balance management mechanism makes it exceedingly difficult. In order to make it easier for the offshore wind farms and the electricity grid to be connected, M3C acts as a LFAC system and frequency changer. M3C balance energy management mechanisms and allow converters to functions in four quadrants with balanced capacitor voltages of Sub-Modules (SM) on the offshore side resuting in reducing frequencies from 50 Hz to 16.7 Hz [18].

Using multilevel conversion, one may build a high-power converter with low-power semiconductors, which has garnered a lot of interest. The basic idea is to use many tiny DC voltages to generate AC voltage waveforms. Smaller voltage steps result in less AC voltage waveform distortion, less switching loss, less voltage change rate (dv/dt) and fewer filter elements needed. Complexity of control and complexity of bus-bar connections are two key drawbacks of multilevel conversion. More semiconductor components are needed. Because lower-rated devices can be utilized, the cost of semiconductors is not increased, but the number of gate-driver circuits needed increases, as does the complexity of the design. The DC-link capacitors also add extra weight and size, which is a disadvantage. The busbar constructions of the multilevel DC-link converter grow more complicated and challenging to build as the number of voltage levels increases.

The neutral point clamped (NPC) and flying capacitor (FC) topologies are two examples of traditional multilevel converters. Multi-level sub modules were also implemented in MMMC [19]. Another arrangement with three voltage states is the cascaded half-bridge submodule (CHBSM). Storage capacitors play pivotal roles in this arrangement of two series-connected half-bridge cells when considering sizes and weights of individual modules. A stackable switching capacitor (SSC) energy buffer in a small submodule topology [20] was developed to do this. SSCSM capacitors can have a minimum 40% less volume than HBSM capacitors. For normal operation, an IGBT is always on and coupled to two additional diodes in a clamp-double submodule (CDSM) [21]. Clamped-double cells can output three separate voltage measurements. In cases of DC failures, all power devices are turned on to stop DC short-circuit currents. CDSM uses only 50% of the available capacitor voltages when in blocking mode. Consequently, CDSM [22] calls for an additional IGBT to be used as a blocking voltage. During typical operation, all of the switches in a CDSM are active; hence this results in higher power losses.

The use of Permanent Magnet Synchronous Generators (PMSG) in large wind turbine generators is on the rise, and PMSG-based WTGs are becoming increasingly common as variable-speed generation systems, since they do not require gearboxes and are connected directly to turbines allowing functioning at low speeds [23–26]. As power electronic technology has evolved, the adoptions of proper generation control systems may reduce weights, losses, costs and demands as well as the need for routine maintenances which are imperative to wind farms. Several varieties of VS-WECS controllers can be found in the research literature [23–28]. They control power, speed and torque through power electronics and aerodynamic mechanisms. The advancement of power electronic devices has also contributed significantly to the enhancement of their controllability and dependability. In addition, there is always a chance of system problems occurring during WTG operation. Short circuit is one of the common problems that can occur. Thus, as more VS-WECS are added to the grid, instability may arise for both the individual systems and the grid as a whole.

A large number of DC sources, semiconductor devices, a high blocking voltage value and other factors that were previously described are thus the key downsides of M3C architectures. In this article, a novel M3C configuration based on a shorter modular module is proposed, this involves few semiconductor devices and DC sources and is appropriate for frequency changers to link offshore wind farms to the power grids through LFAC technology. Different operational circumstances are used to test the proposed M3C technique. The remaining sections are arranged as follows: The topology of the circuit is shown in Section 2. Sections 3 and 4 discuss the operational philosophy, control strategy and sub-control system of the proposed M3C. The simulation results are provided for various operating situations in Section 5 and completed in Section 6 to help validate the effectiveness of the proposed system.

Selected simulation results for various operating situations are used in Section 5 to verify the efficacy of the suggested system. In Section 6, the project is concluded.

2. Circuit topology of M3C

The schematic representation of M3C, which acts as interfaces between two power systems operating at various frequencies as shown in Figure 1. The offshore wind farm (16.7 Hz) is linked to M3C's inputs in this study, and capital letters represent three-phase voltages and currents there: e_A and I_A; e_B and I_B; e_C and I_C respectively. M3C's Three-phase output voltages and currents are represented in lowercases i.e. e_a and I_a; e_b and I_b; e_c and I_c respectively, where outputs of M3Cs are connected to on-shore grids (50 Hz).

The numbering sequences of arms are determined by three phases of inputs and outputs. The input sides of arms are identified as x according to phases A, B and C, respectively (i.e. x = A, B, C). The arm phase output a, b and c are shown as y and analogous to inputs, with

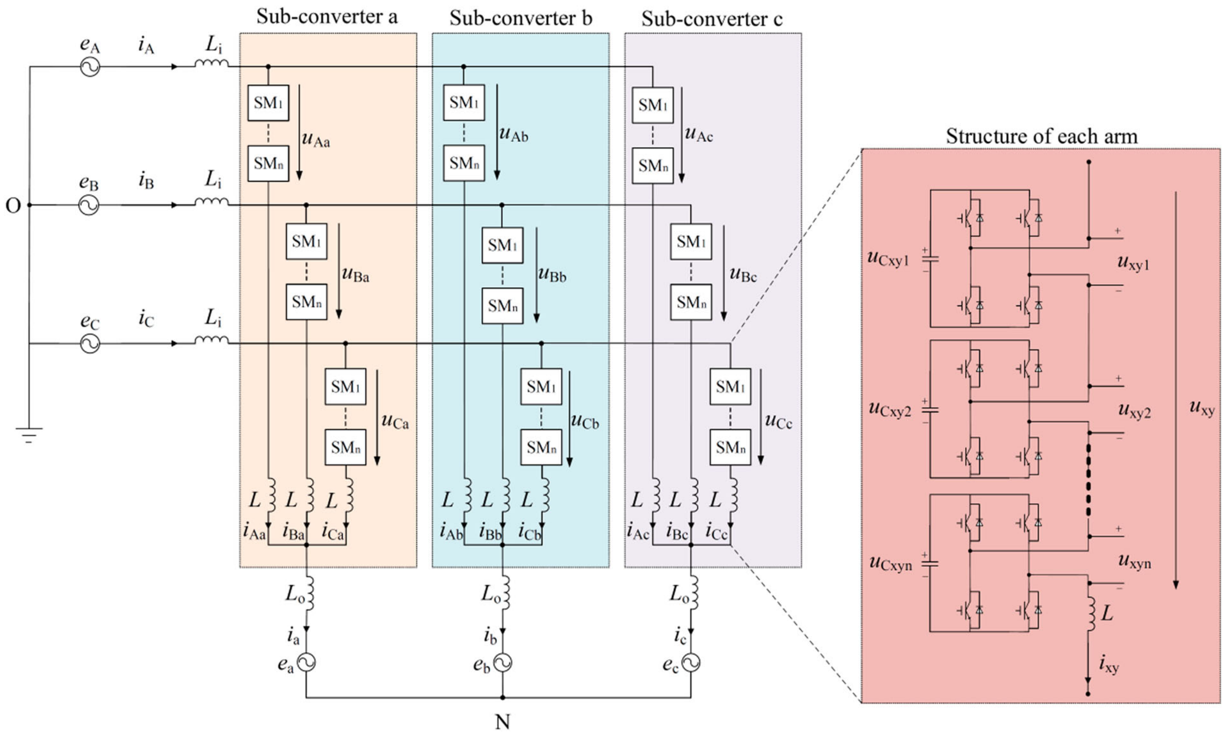

Figure 1. Circuit diagram of modular multilevel matrix converter.

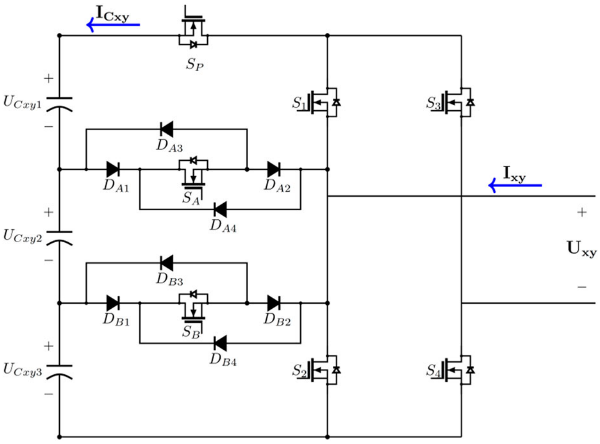

Figure 2. Circuit diagram of proposed M3C converter.

y = a, b and c. Each arm in M3C is denoted by the symbols armxy, i_{xy} and u_{xy}, respectively, for the associated arm's arm current and arm voltage. A series connection between number of SMs and an arm inductor exists in each arm. Seven IGBT switches with related antiparallel diodes, three dc capacitors, and a suggested multilayer converter are used to build each SM. C_{xyz}, where z = 1, 2, 3, are capacitances of SM capacitors. For each SM shown in Figure 2, the three possible u_{xyz}'s output voltage levels are uC_{xyz}, 0 and $-uC_{xyz}$, where the four IGBT switches' statuses are responsible.

The energy regulation in the M3 C capacitors is studied using a single branch similar to that shown in Figure 1. The amount of energy stored in cells branches can be described as integrals of powers at their terminals, ignoring internal losses. The energy of a branch is also proportional to the voltages across its capacitors. Thus, the capacitor voltage may be calculated from the branch current:

$$U_{xy} = \int P_{xy}dt \approx \frac{nC}{2}\bar{V}_C^2 \rightarrow P_{xy} \approx nC\overline{v_C}^0 \frac{d}{dt}(\overline{V_C}) \tag{1}$$

where $x \in \{A-B-C\}$, $y \in \{a-b-c\}$, P_{xy} represents the branch power. $\overline{V_C}$ is the cluster average capacitor voltage, $\overline{V_C}^0$ is the t desired voltage in each cell, the point, n represents cells counts, C stands for capacitors' capacitances and U_{xy} symbolize total energies in n capacitors.

The first step is to adjust the coordinates of input systems (A-B-C) such that they fit into the frame of reference. After then, the systems at the output undergo a transformation into the frame of reference. The corresponding circuit as perceived by the output corresponds to the zero sequence component of V_{Ay}, V_{By} and V_{CY}. This input equivalent circuit can be used to get the zero sequence part of V_{xa}, V_{xb} and V_{xc}, and similarly. Since no path is taken into account, the current flowing between nodes N and n is 0. Input, converter, and output of the M3C can be modelled independently using the following equations:

$$\begin{bmatrix} V_{s\alpha} \\ V_{s\beta} \end{bmatrix} = \begin{bmatrix} V_{\alpha 0} \\ V_{\beta 0} \end{bmatrix} + L_{11}\frac{d}{dt}\begin{bmatrix} i_{s\alpha} \\ i_{s\beta} \end{bmatrix} \tag{2}$$

$$\begin{bmatrix} V_{g\alpha} \\ V_{g\beta} \end{bmatrix} = \begin{bmatrix} V_{0\alpha} \\ V_{0\beta} \end{bmatrix} + L_{22}\frac{d}{dt}\begin{bmatrix} i_{g\alpha} \\ i_{g\beta} \end{bmatrix} \tag{3}$$

$$\begin{bmatrix} V_{\alpha\alpha} & V_{\beta\alpha} \\ V_{\alpha\beta} & V_{\beta\beta} \end{bmatrix} = -L_b\frac{d}{dt}\begin{bmatrix} i_{\alpha\alpha} & i_{\beta\alpha} \\ i_{\alpha\beta} & i_{\beta\beta} \end{bmatrix} \tag{4}$$

where

$$L_{11} = (L_1 + L_b/3) \tag{5}$$

$$L_{22} = (L_2 + L_b/3) \tag{6}$$

The dynamics of the M3C are represented by the system defined by Equations (2)–(4). You can think of (2) and (3) as the input and output systems. In (4), circulating currents within converters are defined accurately resulting in no changes to input and output currents while controlling circulating currents.

3. Working principle proposed M3C converter

The difference in capacitor voltage directly relates to each SM's instantaneous power. The dc capacitors of SM have three states namely charging, discharging and bypassed based on switching states of IGBT switch and directions of arm currents, as shown in Table 1.

Figure 3 illustrates the operation when S_1, S_4, S_2, S_3, S_A and S_B are switched on and off, respectively, the proposed inverters are connected to arms for generating output voltages U_C and $-U_C$ respectively. When there is negative current Switch S_P is OFF and capacitors discharge through Switches S_1, S_4 as shown in Figure 3(a). Hence, when the current is positive the Switch S_P is on and flows through anti-parallel diodes of S_1, S_4 and capacitors are charged as depicted in Figure 3(b).

As shown in Figure 4, when S_A, S_4 are active and turned on S_2, S_3, S_1, S_B are turned off, the arm is attached to the suggested inverter, and its output voltage

Table 1. Switching states of SM in proposed M3C.

State	S1	S2	S3	S4	SA	SB	SP	Ixy	Pxy	Uxy	Cxy1	Cxy2	Cxy3
1	ON	OFF	OFF	ON	OFF	OFF	ON	< 0	< 0	Ucxy	Discharge	Discharge	Discharge
2	ON	OFF	OFF	ON	OFF	OFF	ON	> 0	> 0	Ucxy	Charge	Charge	Charge
3	OFF	OFF	OFF	ON	ON	OFF	OFF	< 0	< 0	2Ucxy/3	Bypass	Discharge	Discharge
4	OFF	OFF	OFF	ON	ON	OFF	OFF	> 0	> 0	2Ucxy/3	Bypass	Charge	Charge
5	OFF	OFF	OFF	ON	OFF	ON	OFF	< 0	< 0	Ucxy/3	Bypass	Bypass	Discharge
6	OFF	OFF	OFF	ON	OFF	ON	OFF	> 0	> 0	Ucxy/3	Bypass	Bypass	Charge
7	OFF	ON	OFF	ON	OFF	OFF	OFF	$> 0/ < 0$	0	0	Bypass	Bypass	Bypass
8	ON	OFF	ON	OFF	OFF	OFF	OFF	$> 0/ < 0$	0	0	Bypass	Bypass	Bypass
9	OFF	OFF	ON	OFF	ON	OFF	ON	> 0	< 0	−Ucxy/3	Discharge	Bypass	Bypass
10	OFF	OFF	ON	OFF	ON	OFF	ON	< 0	> 0	−Ucxy/3	Charge	Bypass	Bypass
11	OFF	OFF	ON	OFF	OFF	ON	ON	> 0	< 0	−2Ucxy/3	Discharge	Discharge	Bypass
12	OFF	OFF	ON	OFF	OFF	ON	ON	< 0	> 0	−2Ucxy/3	Charge	Charge	Bypass
13	OFF	ON	ON	OFF	OFF	OFF	ON	> 0	< 0	−Ucxy	Discharge	Discharge	Discharge
14	OFF	ON	ON	OFF	OFF	OFF	ON	< 0	> 0	−Ucxy	Charge	Charge	Charge

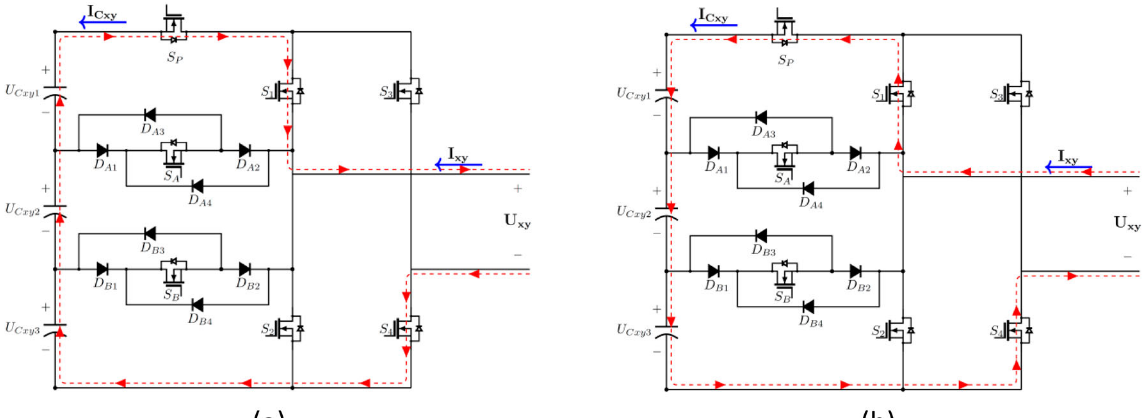

(a) (b)

Figure 3. Status of proposed M3C converter at output $+U_C$.

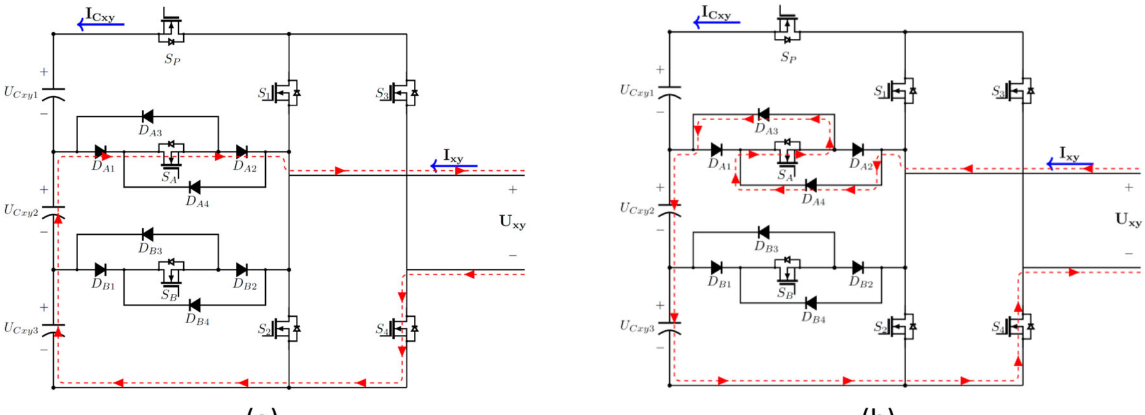

(a) (b)

Figure 4. Status of proposed M3C converter at output $+2U_C/3$.

is $+2U_C/3$. In the Figure 4(a), if the capacitor is present, the current is negative is being discharged through S_A, S_4 Corresponding diode D_{A3}&D_{A4}. Hence, for positive currents, they flow through the anti-parallel diode of switch S_4, switch S_A Corresponding diode D_{A1}&D_{A2} and Figure 4(b) depicts the capacitor being charged.

As shown in Figure 5, when S_B, S_4 are active and turned on S_2, S_3, S_1, S_A are turned off, the suggested inverter is connected with arms with $+U_C/3$ as the output voltage. In the Figure 5(a), if the capacitor is present, the current is negative is being discharged through S_B, S_4 Corresponding diode D_{B3}&D_{B4}. Hence, for positive currents, they flow through the anti-parallel diode of Switch S_4, Switch S_B Corresponding diode D_{B1}&D_{B2} and Figure 5(b) depicts the capacitor being charged.

As Figure 6(a), when S_2 and S_4 are turned on but S_1 and S_3 are off, SM is bypassed with zero output voltage. S1 and S3 are on in Figure 6 while S2 and S4 are off (b). Regardless of the current flowing, its output voltage is zero.

As shown in Figure 7, when S_A, S_3 are active and turned on S_1,S_2,S_4, S_B are turned off, the arm is

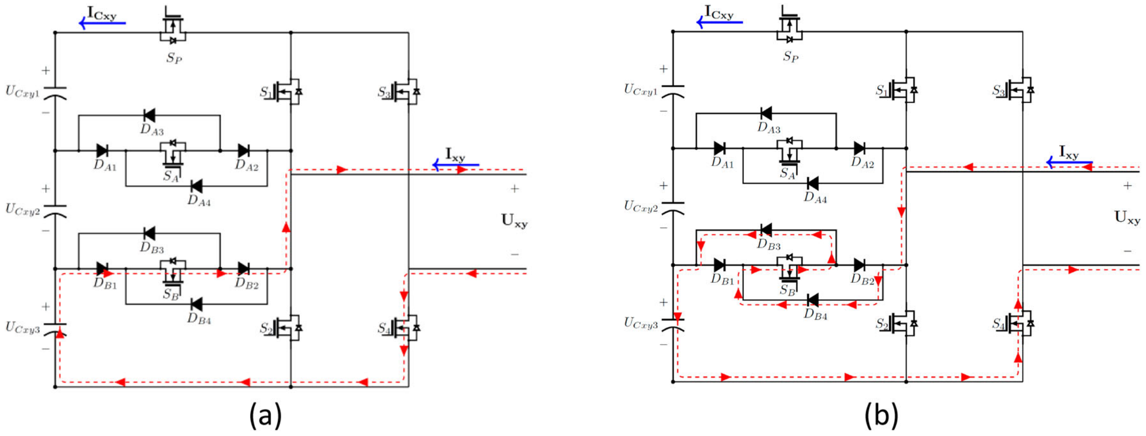

Figure 5. Status of proposed M3C converter at output $+U_C/3$.

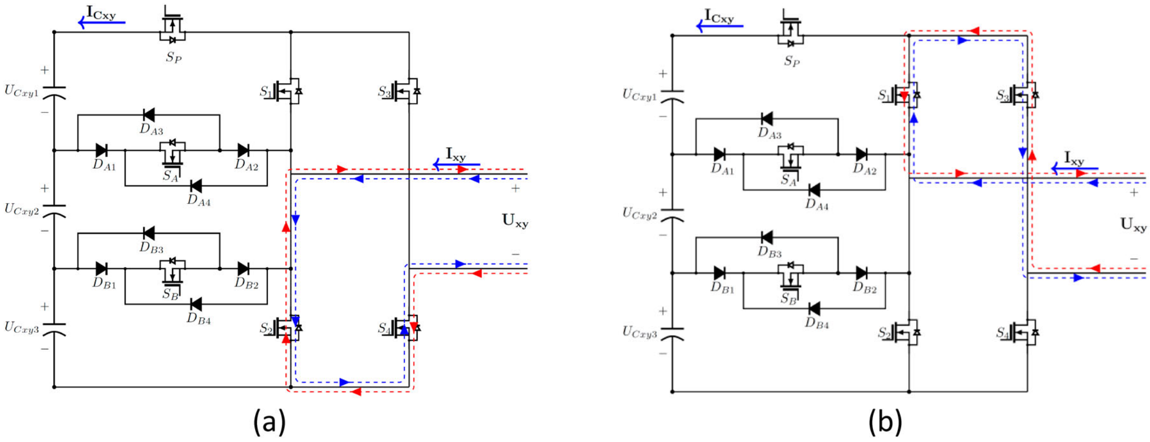

Figure 6. Status of proposed M3C converter at output $+0U_C$.

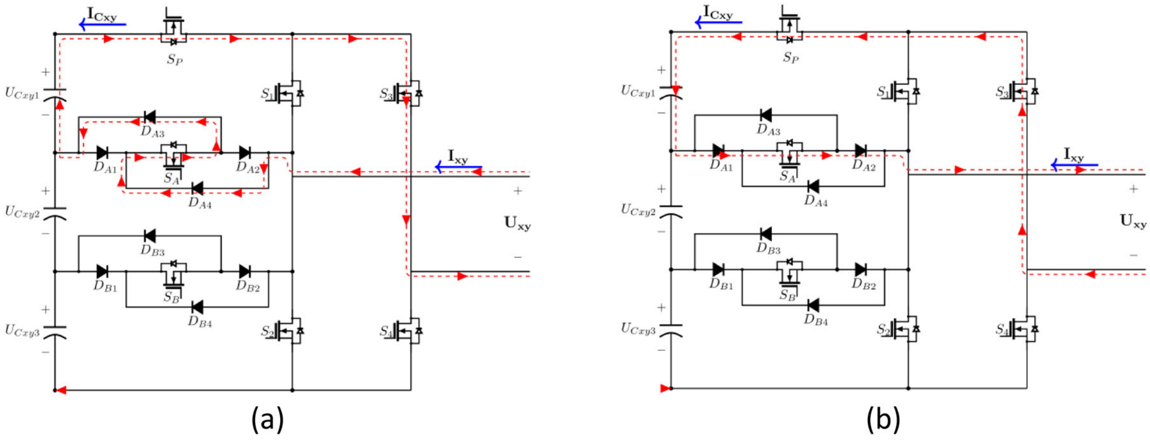

Figure 7. Status of proposed M3C converter at output $-U_C/3$.

attached to the suggested inverter, and its output voltage is $-U_C/3$. In Figure 7(a), switch S_N is OFF for negative currents and capacitors are being discharged through S_A, S_3, corresponding diode D_{A3}&D_{A4}. Therefore, when the current is positive switch S_P is ON and it flows through the antiparallel diode of Switch S_3, Switch S_A Corresponding diode D_{A1}&D_{A2} and Figure 7(b) depicts the capacitor being charged.

As shown in Figure 8, when S_B, S_3 are active and turned on S_1,S_2, S_4, S_A are turned off, the arm is attached to the suggested inverter, and its output voltage is $-2U_C/3$. In Figure 8(a), S_P is OFF for negative current and the capacitor is being discharged through S_B, S_3 Corresponding diode D_{B3}&D_{A4}. Therefore, for positive current, switch S_P is ON and current flows through anti-parallel diode of Switch S_3, Switch S_B Corresponding diode D_{B1}&D_{B2} Figure 8(b) depicts the capacitor being charged.

As shown in Figure 9, when S_2, S_3 are active and turned on S_1, S_4, S_A, S_B are turned off, the arm is attached to the suggested inverter, and its output voltage is $-U_C$. In the Figure 9(a), when the current is negative Switch S_P is OFF and the capacitor is being discharged through Switch S_3, S_2. Therefore, when the current is positive Switch S_P is on and it flows through the antiparallel diode of S_3, S_2 and Figure 9(b) depicts the capacitor being charged.

4. Double $\alpha\beta 0$ transformation control technique

The block diagram for the "double $\alpha\beta 0$ transformation" control mechanism is shown in Figure 10. The circulating current control loop comes after the input, output, and loop. The reference value u_{xy}^* of the nine arms is determined by computing the reference value of the nine arm voltages in the $\alpha\beta 0$ frame and twice performing the inverse 0 transformation. The PWM [29] signals are ultimately produced by the modulation process. The capacitor voltage control [30] is made up of two parts: the capacitor voltage control overall and the capacitor voltage balancing control. The total capacitor voltage control is computed using the reference value of the input current. Reference values for the four circulating currents are established for the capacitor voltage balancing control. The double $\alpha\beta 0$ to the nine arm currents, transformation has been done, i_{xy}. The eight components of the arm current are then calculated using these. Due to the perfect decoupling of the input, output, and circulating currents, the eight

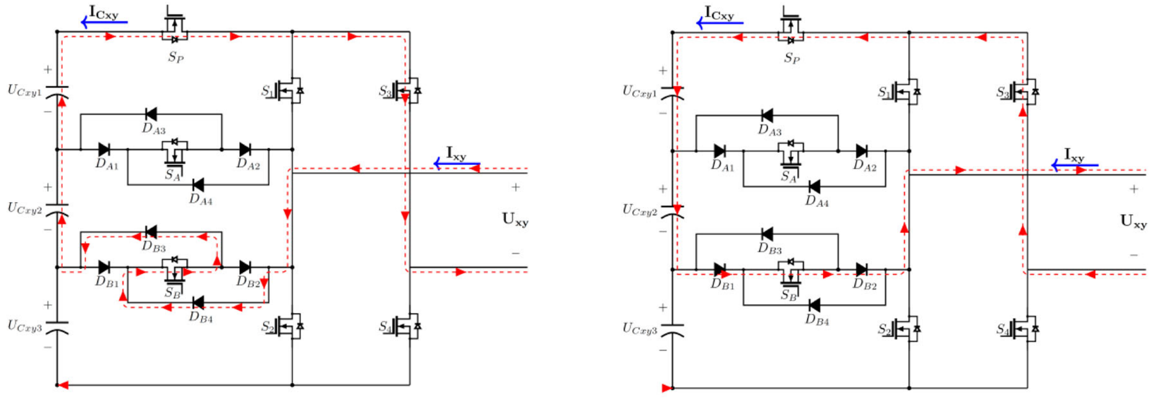

(a) (b)

Figure 8. Status of proposed M3C converter at output $-2U_C/3$.

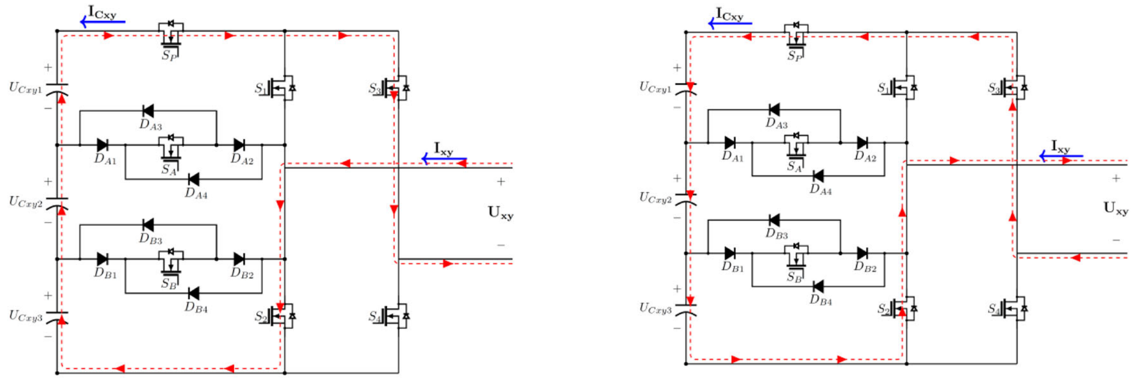

(a) (b)

Figure 9. Status of proposed M3C converter at output $-U_C$.

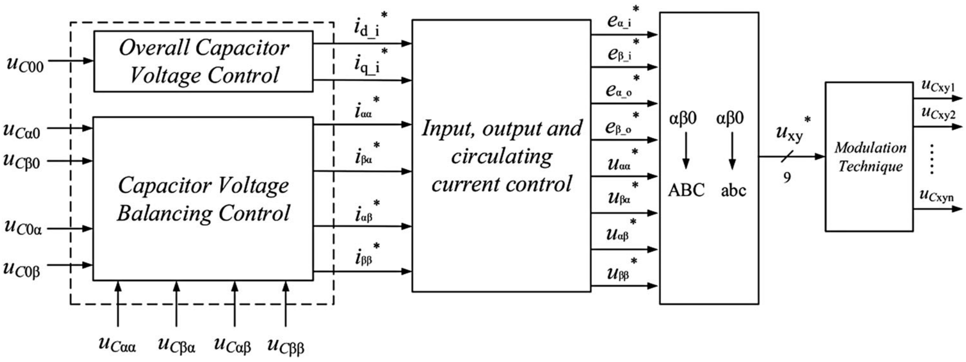

Figure 10. Block diagram of "double $\alpha\beta 0$ transformation" control.

voltage components in the 0 frame are computed using the reference values of these three currents. In conclusion, PWM singles are produced using the modulation approach. Due to the connection between the grid and the output, the control theory is quite similar to input current control.

Mathematically arm$_{\mathrm{Aa}}$ can be formulated as:

$$\left\{ \begin{array}{l} u_{xa} = \sum\limits_{z=1}^{N} u_{xaz} \\ u_{cxa} = \sum\limits_{z-1}^{N} u_{cxaz} \end{array} \right\} \tag{7}$$

Differential of u_{cxy} can be formulated as:

$$\frac{du_{cxa}}{dt} = \sum_{z=1}^{N} \left(\frac{p_{xaz}}{u_{cxaz}} . \frac{1}{C_{xaz}} \right) \tag{8}$$

It is fair to assume that during steady operation, the capacitance and capacitor voltage in M3C are same. Therefore:

$$\left\{ \begin{array}{c} u_{Cxa} = n.u_{Cxaz} \\ P_{xa} = n.P_{xaz} \end{array} \right\} \tag{9}$$

Hence, Equation (7) could be further simplified as:

$$\frac{du_{cxa}}{dt} = \frac{n}{C_{xa7}} . \frac{P_{xaz}}{u_{Cxa7}} = \frac{n}{C_{xa7}} . \frac{P_{xa}}{u_{Cxa}} \tag{10}$$

From Equation (10), we know that arm Aa's capacitors are being charged whenever $p_{xa} < 0$ and the corresponding $\frac{du_{cxa}}{dt} > 0$. The capacitors in arm Aa are charged when $p_{xa} < 0$and discharged when $p_{xa} < 0$. Therefore, in order to get voltage equilibriums in the capacitors:

$$w_{xa} = \int_{t}^{t+T} p_{xa} dt = 0 \tag{11}$$

Since capacitors can only store reactive power, this implies that active power must be zero. The arm Aa capacitor voltage is assumed to be equal parts dc capacitor voltage U_{Cxa} and ac variation U_{Cxa}, with $u_{Cxa} \ll U_{Cxa}$.

$$\begin{aligned} u_{Cxa} &= U_{Cxa} + u_{Cxa} \approx U_{Cxa} + \frac{n}{C.U_{Cxa}} . \int_{t}^{t+T} p_{xa} dt \\ &= U_{Cxa} + \frac{n}{C.U_{Cxa}} . \int_{t}^{t+T} u_{xa} i_{xa} dt \end{aligned} \tag{12}$$

Equation (12) describes the relationship between the arm's active power and the u_{Cxy}:

$$\begin{aligned} &\begin{bmatrix} u_{CAa} & u_{CBa} & u_{CCa} \\ u_{CAb} & u_{CBb} & u_{CCb} \\ u_{CAc} & u_{CBc} & u_{CCc} \end{bmatrix} \\ &= \frac{n}{CU_{Cxy}} \int \begin{bmatrix} p_{Aa} & p_{Ba} & p_{Ca} \\ p_{Ab} & p_{Bb} & p_{Cb} \\ p_{Ac} & p_{Bc} & p_{Cc} \end{bmatrix} dt \\ &+ U_{Cxy} * \begin{bmatrix} 1 & 1 & 1 \\ 1 & 1 & 1 \\ 1 & 1 & 1 \end{bmatrix} \end{aligned} \tag{13}$$

The same "double $\alpha\beta 0$ transformation" is the applied to Equation (13) to give:

$$\begin{aligned} &\begin{bmatrix} u_{C\alpha\alpha} & u_{C\beta\alpha} & u_{C0\alpha} \\ u_{C\alpha\beta} & u_{C\beta\beta} & u_{C0\beta} \\ u_{C\alpha 0} & u_{C\beta 0} & u_{C00} \end{bmatrix} \\ &= \frac{n}{CU_{Cxy}} \int \begin{bmatrix} p_{\alpha\alpha} & p_{Ba} & p_{0\alpha} \\ p_{\alpha\beta} & p_{Bb} & p_{0\beta} \\ p_{\alpha 0} & p_{\beta 0} & p_{00} \end{bmatrix} \mathrm{dt} \\ &+ \begin{bmatrix} 0 & 0 & 0 \\ 0 & 0 & 0 \\ 0 & 0 & 3U_{Cxyz} \end{bmatrix} \end{aligned} \tag{14}$$

where $u_{C\alpha\alpha}, u_{C\beta\alpha}, \ldots, u_{C00}$ represent corresponding $\alpha\beta 0$ components of $u_{CAa}, u_{CBa}, \ldots, u_{CCc}$. $p_{\alpha\alpha}, p_{\beta\alpha}, p_{00}$ are corresponding $\alpha\beta 0$ components of p_{Aa}, p_{Ba}, p_{Cc}.

Mathematical relationships between arm powers, arm voltages and arm currents can be computed using mathead software as detailed below:

$$p\alpha\alpha = \frac{1}{3}(e_{\alpha\_i} i_{\alpha\_0} - i_{\alpha\_i} e_{\alpha\_0})$$

$$\begin{aligned}&+\frac{1}{\sqrt{6}}(e_{\alpha\_i}i_{\alpha\alpha}-e_{\beta\_i}i_{\beta\alpha})\\&-\frac{1}{\sqrt{6}}(e_{\alpha\_0}i_{\alpha\alpha}-e_{\beta\_0}i_{\beta\alpha})\end{aligned}\tag{15}$$

$$\begin{aligned}\mathrm{p}\beta\alpha=&\frac{1}{3}(e_{\beta\_i}i_{\alpha\_0}-i_{\alpha\_i}e_{\alpha\_0})\\&-\frac{1}{\sqrt{6}}(e_{\alpha\_i}i_{\beta\alpha}+e_{\beta\_i}i_{\alpha\alpha})\\&-\frac{1}{\sqrt{6}}(e_{\alpha\_0}i_{\beta\alpha}-e_{\beta\_0}i_{\beta\beta})\end{aligned}\tag{16}$$

$$\begin{aligned}\mathrm{p}0\alpha=&\frac{1}{\sqrt{3}}(e_{\alpha\_i}i_{\beta\alpha}-e_{\beta\_i}i_{\alpha\alpha})\\&-\frac{\sqrt{2}}{\sqrt{6}}(e_{\alpha\_0}i_{\alpha\_0}-e_{\beta\_0}i_{\beta\_0})\end{aligned}\tag{17}$$

$$\begin{aligned}\mathrm{p}\alpha\beta=&\frac{1}{3}(e_{\alpha\_i}i_{\beta\_0}-i_{\alpha\_i}e_{\beta\_0})\\&+\frac{1}{\sqrt{6}}(e_{\alpha\_i}i_{\alpha\beta}+e_{\beta\_i}i_{\beta\beta})\\&+\frac{1}{\sqrt{6}}(e_{\alpha\_0}i_{\alpha\beta}+e_{\beta\_0}i_{\alpha\alpha})\end{aligned}\tag{18}$$

$$\begin{aligned}\mathrm{p}\beta\beta=&\frac{1}{3}(e_{\beta\_i}i_{\beta\_0}-i_{\beta\_i}e_{\beta\_0})\\&-\frac{1}{\sqrt{6}}(e_{\alpha_i}i_{\beta\beta}+e_{\beta_i}i_{\alpha\beta})\\&+\frac{1}{\sqrt{6}}(e_{\alpha\_i}i_{\beta\beta}+e_{\beta\_0}i_{\beta\alpha})\end{aligned}\tag{19}$$

$$\begin{aligned}\mathrm{p}\alpha\beta=&\frac{1}{\sqrt{3}}(e_{\alpha\_i}i_{\alpha\beta}+e_{\beta\_i}i_{\beta\beta})\\&+\frac{\sqrt{2}}{\sqrt{6}}(e_{\alpha\_0}i_{\beta\_0}+e_{\beta\_0}i_{\alpha\_0})\end{aligned}\tag{20}$$

$$\begin{aligned}\mathrm{p}\alpha0=&\frac{\sqrt{2}}{6}(e_{\alpha\_i}i_{\alpha\_i}-e_{\beta\_i}i_{\beta\_i})\\&-\frac{1}{\sqrt{3}}(e_{\alpha\_0}i_{\alpha\alpha}+e_{\beta\_0}i_{\alpha\beta})\end{aligned}\tag{21}$$

$$\begin{aligned}\mathrm{p}\beta0=&-\frac{\sqrt{2}}{6}(e_{\alpha\_i}i_{\beta\_i}+e_{\beta\_i}i_{\alpha\_i})\\&-\frac{1}{\sqrt{3}}(e_{\alpha\_0}i_{\beta\alpha}+e_{\beta\_0}i_{\beta\alpha})\end{aligned}\tag{22}$$

$$\mathrm{p}00=\frac{1}{3}(e_{\alpha\_i}i_{\beta\_i}+e_{\beta\_i}i_{\beta\_i}-e_{\alpha_0}i_{\alpha_0}-e_{\beta\_0}i_{\beta\_0})\tag{23}$$

Therefore Equations (15)–(23) show the computations for active power of nine arms in the $\alpha\beta0$ frame.

The values of the parameters p0, p0, p0 and p0 establish overall energy balances of sub-converters. The parameters p, p, p, p. p00 govern the total energy consumption and consumption rate of M3C's, while p, p, p, p. p00 regulate the energy equilibrium between arms of sub converters.

Capacitor voltage control

The regulation of capacitor voltage consists of two subsystems: global regulation and voltage balancing. Reference values for the four circulating currents are calculated using Equations (23) and (14), and this information is then used to regulate the capacitor voltage as a whole. In the sections that follow, we'll go deeper into the control strategy's specifics.

Reference DC values of $u_{c\alpha\alpha}$, $u_{c\beta\alpha}$, … ., $\mathrm{u_{c00}}$ should be controlled from:

$$\begin{bmatrix}U_{C\alpha\alpha} & U_{C\beta\alpha} & U_{C0\alpha}\\ U_{C\alpha\beta} & U_{C\beta\beta} & U_{C0\beta}\\ U_{C\alpha0} & U_{C\beta0} & U_{C00}\end{bmatrix}=\begin{bmatrix}0 & 0 & 0\\ 0 & 0 & 0\\ 0 & 0 & 3U_{Cxyz}\end{bmatrix}\tag{24}$$

where $U_{C0\alpha}$, $U_{c\beta\alpha}$, … … , U_{C00} represents the corresponding DC value of $u_{C0\alpha}$, $u_{c\beta\alpha}$, … … , u_{C00}.

Overall capacitor voltage controls implies controlling $U_{C00}=3U_C^*$. Hence, P_{00} is controlled using P controller as:

$$P_{00}*=3K1\left(U_{Cxy}*-\frac{U_{C00}}{3}\right)\tag{25}$$

where p_{00}^* is the reference value of p_{00}. K_1 is the gain of the P controller.

Equation (10) is used to calculate the input current, which is then converted to a dq frame:

$$\begin{aligned}\sqrt{3}\begin{bmatrix}e_{d\_i}\\ e_{q\_i}\end{bmatrix}=&\frac{1}{\sqrt{3}}\begin{bmatrix}L\frac{d}{dt} & -\omega_iL\\ \omega L & L\frac{d}{dt}\end{bmatrix}\begin{bmatrix}i_{d\_i}\\ i_{q\_i}\end{bmatrix}\\&+\begin{bmatrix}e_{d\_0}\\ e_{q\_0}\end{bmatrix}\end{aligned}\tag{26}$$

Hence, P_{00} is calculated from:

$$P_{00}=\frac{1}{3}e_{d\_i}i_{d\_i}-\frac{1}{3}(e_{\alpha_0}i_{\alpha_0}+e_{\beta\_0}i_{\beta\_0})\tag{27}$$

where input powers of $\mathrm{M^3C}$ are defined by $p_i{:}p_i=e_{d\_i}i_{d\_i}$ and output powers of M3C are defined by $p_0{:}p_0=e_{a\_0}i_{\alpha\_0}+e_{\beta\_0}i_{\beta\_0}$

Hence, reference values of input currents $i_{d\_i}^*$ are computed from:

$$i_{d\_i}^*=\frac{p_0^*}{e_{d\_i}}+K_2\left(1+\frac{1}{ST_2}\right)\left(U_{Cxy}^*-\frac{U_{C00}}{3}\right)\tag{28}$$

where p_0^* refers to reference values of output powers while K_2 stands for proportional gains and T_2 represents sampling time.

Then $i_{q\_i}^*$ is equal to zero for the unity power factor.

$$i_{q\_i}^*=0\tag{29}$$

The wind turbine grid-side converter uses a virtual synchronizer-based grid-forming control to maintain system frequency and regulate active and reactive power transmission on the grid side, as shown in Figure 11. The inertia and damping characteristics

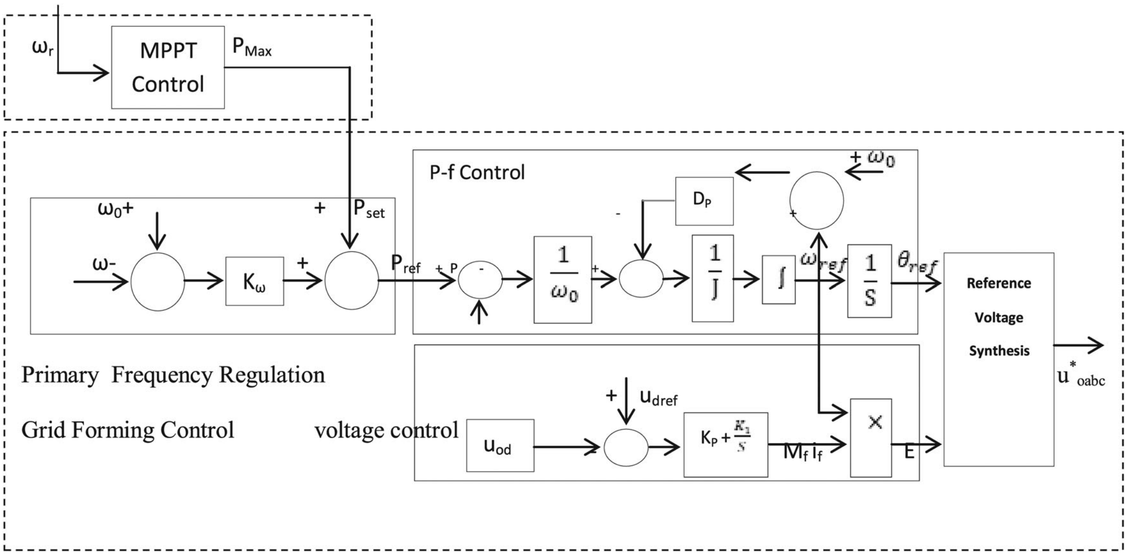

Figure 11. PMSG wind turbine grid-forming control.

of actual synchronous generators are simulated by a virtual synchronous generator's frequency dynamics, which are based on conventional oscillation equations.

$$\left\{\begin{aligned} \frac{d\omega_{\text{ref}}}{dt} &= \frac{1}{J}\left[\frac{P_{\text{ref}}}{\omega_0} - \frac{P}{\omega_0} - D_P(\omega_{\text{ref}} - \omega_0)\right] \\ \frac{d\theta_{\text{ref}}}{dt} &= \omega_{\text{ref}} \end{aligned}\right\} \tag{30}$$

In the given context, P represents the effective active power generated by the grid-side inverter. Pref denotes the reference values for active powers on grids. J signifies the virtual inertia of the rotor's rotation, while Dp represents the damping factor. The rated angular frequency is represented by the number 0. Ref stands for both the reference value for the phase of the AC-side voltage and the reference value for the produced angular frequency. When J/Dp is less than zero, the grid-side converter uses DC voltage external loop control to maintain operating in a unit power factor state. The DC bus voltage is stabilized as a result, and the reference value of reactive current is set to zero. Equation displays the relevant control equations for the D- and q-axis currents for given input values.

$$\left\{\begin{aligned} i_{gd}^{*} &= \left(K_P + \frac{K_I}{s}\right)(U_{dc}^{*} - U_{dc}) \\ i_{gq}^{*} &= 0 \end{aligned}\right\} \tag{31}$$

where K_p, K_I represent the proportional and integral adjustments to the inner loop respectively. The values of the current i_{gd}^* and i_{gq}^* are denoted by i_{gd} and i_{gq}, respectively. The DC bus voltage, denoted by $U_{dc}^* i_s$, has a set value.

5. Simulation results and discussion

MATLAB/SIMULINK software was used to simulate the suggested M3C using the "double $\alpha\beta 0$ transformation" technique. The 16.7 Hz offshore wind farm is linked to the input side of M3C, while the Grid is connected to the output side of the M3C (50 Hz). Table 2 shows the parameters considered for simulation.

Table 2. Simulation parameters of the proposed M3C.

Parameters	Value
PMSG wind turbine power (P_{ABC})	
PMSG wind turbine line voltage (V_{ABC})	690 V
PMSG wind turbine rated frequency (F_{ABC})	16.7 Hz
Grid side line voltage (V_{abc})	690 V
Grid side frequency (F_{abc})	50 Hz
Arm inductance (L_i&L_o)	1 mH
Switching frequency (F_{SW})	20 Khz
Capacitance of SM's capacitor (C_{xy1}, C_{xy2}&C_{xy3})	220 uF
No of SM capacitor per leg	3
Rated DC capacitor voltage (U_{cxy})	1200 V

Figure 12(a,b) demonstrates the outcomes of simulating the proposed M3C in steady state operation. The operation of the unity power is demonstrated by the input voltage and input current of the PMSG wind production at 16.7 Hz being in phase. Figure 12(c,d) display the grid side's output voltage and current at 50 Hz, illustrative of unity power. Figure 13 depicts the equivalent output load power of 2.09 Kw and the associated input PMSG wind power of 2.18 Kw.

Two frequency components, 50 and 16.7 Hz, are present in the arm current depicted in Figure 14(a). Figure 14(b) displays the armAa voltages across the three capacitors. The identical capacitor voltages in sub-converter arms Aa, Ba and Ca show a constant energy gap between them. Graph 14(c).

Figure 15(a) shows the wind speed constant of 15 m/s as a reference to generate the corresponding output power. The corresponding PMSG torque and speed are shown in Figure 15(b,c) respectively.

As shown in the Table 3. The proposed M3C converter consists of 63 switches with much lower than the

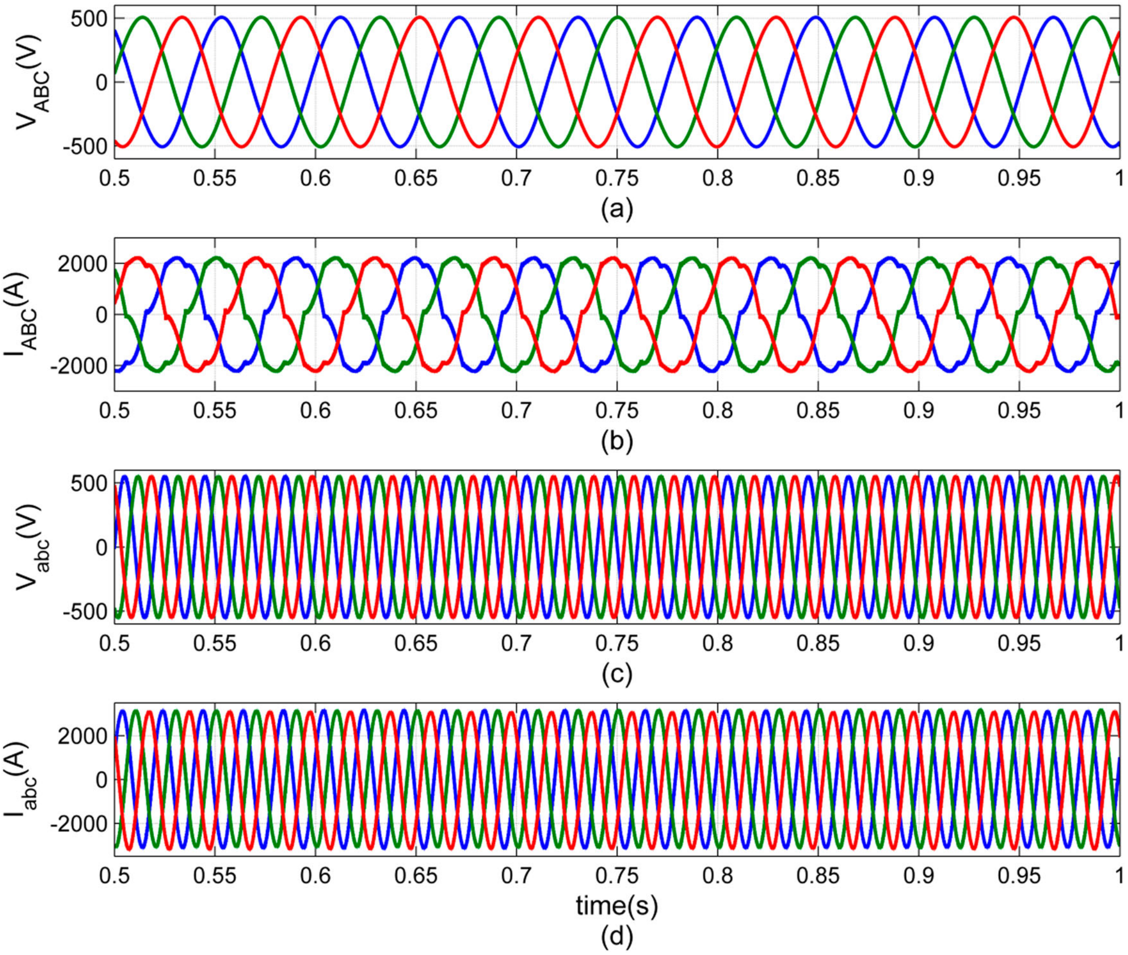

Figure 12. Simulation input/output voltage and current wave form of proposed M3C.

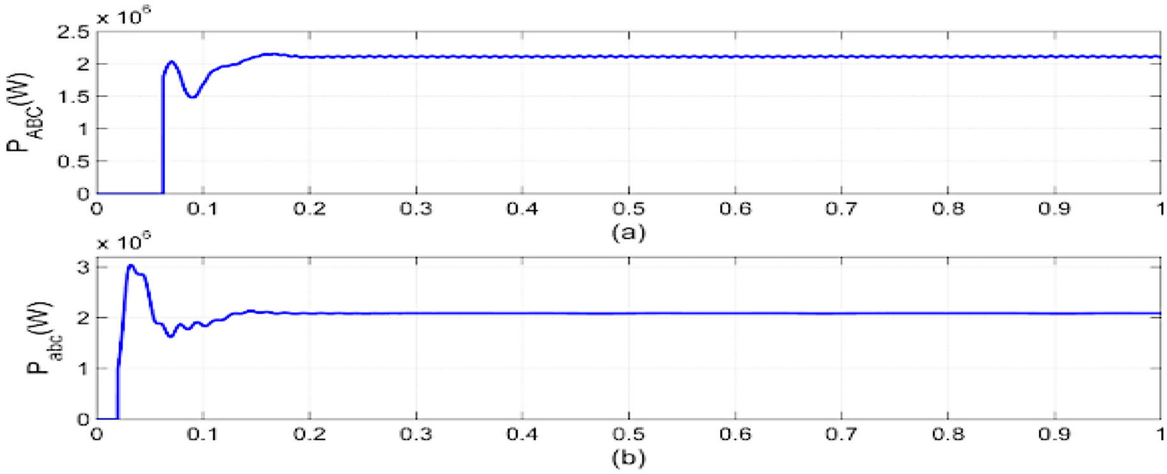

Figure 13. Simulation Input/output power wave form of proposed M3C.

Table 3. Comparison table of SM M3C converter and proposed M3C converter.

Parameter	Levels	DC source	DC capacitor	Switches	Diode
SM M3C converter	7	27	27	108	0
Proposed M3C converter	7	9	27	63	72

exiting SM M3C converter. Thus, the switching losses and conductive losses of MOSFET is reduced which improves the efficacy of the proposed converter. The cost and size of the system is reduced due to the less number of MOSFET and driver Component. Proposed M3C converter uses 72 diodes instead of MOSFET. Hence less switching losses will increases the efficiency.

6. Conclusion

This article examined the performance of an M3C converter for low frequency operation in an offshore LFAC application. The power control and capacitor

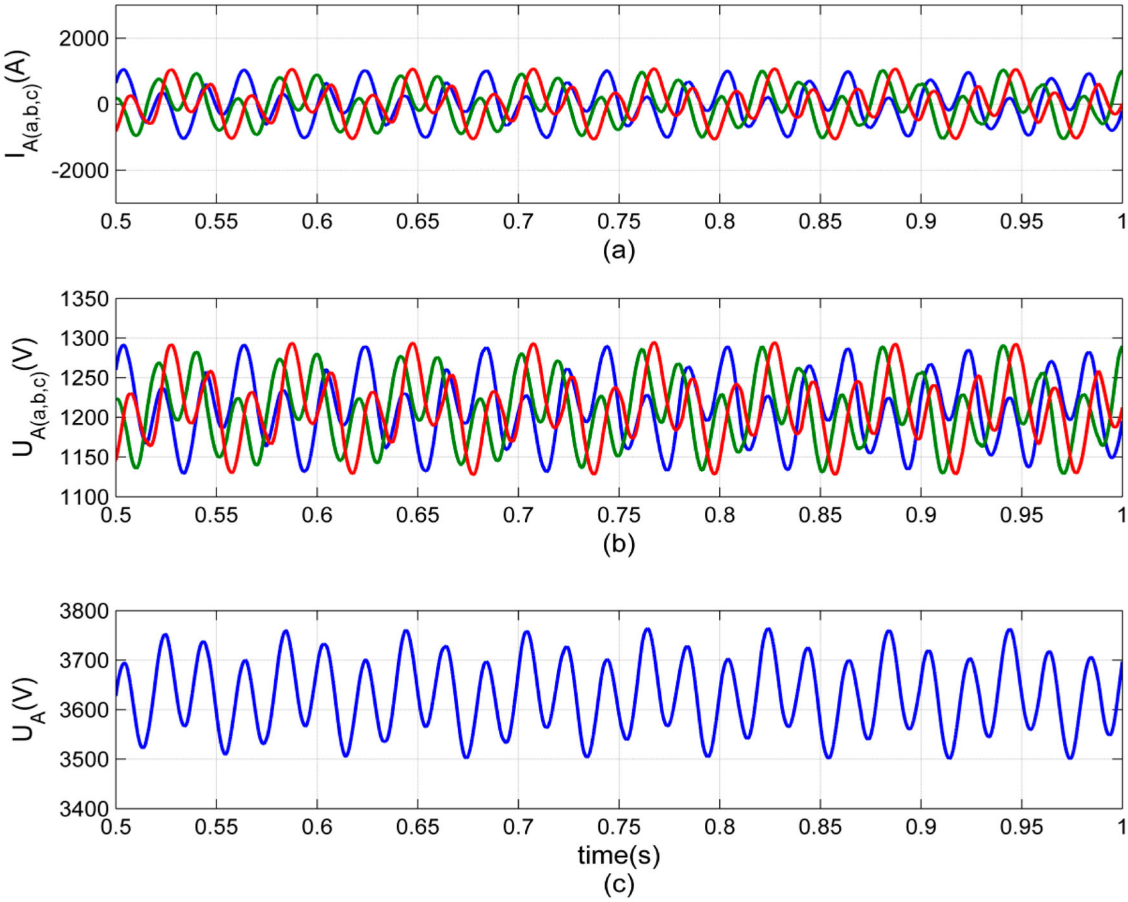

Figure 14. Arm current and capacitor voltage of proposed M3C.

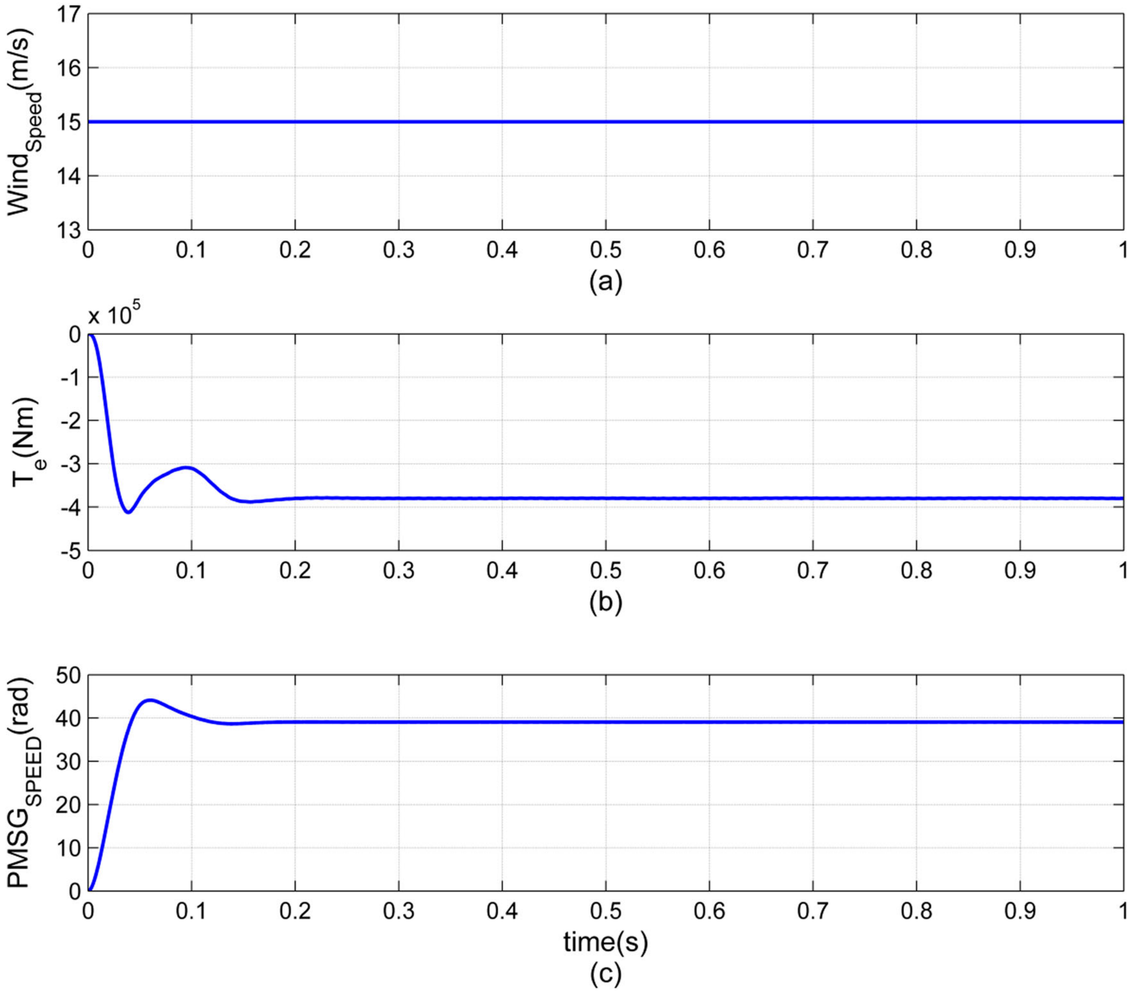

Figure 15. PMSG wind turbine wave form of proposed M3C.

voltage balance control techniques for the M3C are provided. Through numerical modelling, the recommended strategies were confirmed. In a system for offshore wind farms, low frequency conversion operations from 16.7 Hz to 50 Hz were demonstrated. This paper includes control of the input current, output current, and circulating current in such applications using double $\alpha\beta 0$ transformation technique. By using a fewer number of switching devices and an energy controller, the proposed M3C method is able to establish voltage and current balance in the SM capacitor throughout a wide range of operating circumstances. The efficiency, compactness, and low cost of the suggested system are readily apparent. The proposed M3C converter for LFAC applications also allows for adaptive grid side control with SVPWM, which can boost grid side performance.

Disclosure statement

No potential conflict of interest was reported by the author(s).

References

[1] Zhou Y, Macpherson DE, Blewitt W, et al. Comparison of DC-DC converter topologies for offshore wind-farm application. In: 6th IET International Conference on Power Electronics, Machines and Drives (PEMD 2012): Bristol; 2012. p. 1–6.

[2] GOV. UK. UK Renewable Energy Roadmap; 2011. Crown copyright 2011, Department of Energy & Climate Change, 3 Whitehall place London SW1A 2AW, www.decc.gov.uk, REF: URN 11D/698.

[3] Liu S, Wang X, Ning L, et al. Integrating offshore wind power via fractional frequency transmission system. IEEE Trans Power Deliv. Jun 2017;32(3):1253–1261. doi:10.1109/TPWRD.2015.2435993

[4] Nakagawa R, Funaki T, Matsuura K. Installation and control of cycloconverter to low frequency AC power cable transmission. In: Conf. Rec. of Power Conversion Conference (PCC-Osaka 2002); 2002, p. 1417–1422.

[5] Qin N, You S, Xu Z, et al. Offshore wind farm connection with low frequency AC transmission technology. In: Conf. Rec. IEEEPES General Meeting; 2009. p. 1–8.

[6] Fischer W, Braun R, Erlich I. Low frequency high voltage offshore grid for transmission of renewable power. 2012 3rd IEEE PES Innovative Smart Grid Technologies Europe (ISGT Europe), Berlin; 2012. p. 1–6.

[7] Hiller M, Krug D, Sommer R, et al. A new highly modular medium voltage converter topology for industrial drive applications. In: EPE '09: 13th European Conference on Power Electronics and Applications, 2009; 2009. p. 1–10.

[8] Yang Qx, Wang W, Xu Lj, et al. Research on wind power connected to power grid by fractional frequency transmission system. In: Power and Energy Engineering Conference (APPEEC), 2010 Asia-Pacific; 2010. p. 1–4.

[9] Debnath S, Saeedifard M. A new hybrid modular multilevel converter for grid connection of large wind turbines. IEEE Trans Sust Energy. 2013;4:1051–1064. doi:10.1109/TSTE.2013.2266280

[10] Gemmell B, Dorn J, Retzmann D, et al. Prospects of multilevel VSC technologies for power transmission. In: Transmissionand Distribution Conference and Exposition, 2008, IEEE/PES; 2008. p. 1–16.

[11] Akagi H. Classification, terminology, and application of the modular multilevel cascade converter (MMCC). IEEE Trans Power Electron. 2011;26(11):3119–3130. doi:10.1109/TPEL.2011.2143431

[12] Zhuo G, Jiang D, Lian X. Modular multilevel converter for unified power flow controller application. In: 2012 Third International Conference on Digital Manufacturing and Automation (ICDMA); 2012. p. 545–549.

[13] Winkelnkemper M, Korn A, Steimer P. A modular direct converter for transformerless rail interties. In: IEEE International Symposium on Industrial Electronics (ISIE), 2010; 2010. p. 562–567.

[14] Meshram PM, Borghate VB. A novel voltage balancing method applied to direct control strategy of MMC-HVDC system. In: International Conference on Advances in Engineering, Science and Management (ICAESM), 2012; 2012. p. 448–452.

[15] Erickson R, Al-Naseem O. A new family of matrix converters. In: Industrial Electronic Society, 2001. IECON'01.The 27th Annual Conference of the IEEE, Vol. 2; 2001. p. 1515–1520.

[16] Angkititrakul S, Erickson R. Control and implementation of a new modular matrix converter. In: Applied Power Electronics Conference and Exposition, 2004, APEC'04.Ninetheenth Annual IEEE, Vol. 2; 2004. p. 813–819.

[17] Kammerer F, Kolb J, Braun M. A novel cascaded vector control scheme for the modular multilevel matrix converter. In: IECON 37th Annual Conference on IEEE Industrial Electronics Society; 2011.

[18] Ma JK, Dahidah M, Pickert V. Modular multilevel matrix converter for offshore low frequency AC transmission system. In: 2017 IEEE 26th International Symposium on Industrial Electronics (ISIE).

[19] Solas E, Abad G, Barrena JA, et al. Modular multilevel converter with different submodule concepts—part I: capacitor voltage balancing method. IEEE Trans Ind Electron. 2013;60:4525–4535. doi:10.1109/TIE.2012.2210378

[20] Tang Y, Chen M, Ran L. A compact MMC submodule structure with reduced capacitor size using the stacked switched capacitor architecture. IEEE Trans Power Electron. 2015;31:1. doi:10.1109/TPEL.2015.2511189

[21] Marquardt R. Modular multilevel converter topologies with DC-short circuit current limitation. In: Proceedings of the 8th International Conference on Power Electronics—ECCE Asia, Jeju, Korea; 29 May–2 June 2011. p. 1425–1431.

[22] Zhang Y, Ravishankar J, Fletcher J, et al. Review of modular multilevel converter based multi-terminal HVDC systems for offshore wind power transmission. Renew Sustain Energy Rev. 2016;61:572–586. doi:10.1016/j.rser.2016.01.108

[23] Errami Y, Ouassaid M, Maaroufi M, et al. Direct torque control and MPPT strategy of PMSG used for variable speed wind energy conversion system. In: IEEE-International Conference on Systems and Control (ICSC); June 2012.

[24] Chen Z, Guerrero JM, Blaabjerg F. A review of the state of the art of power electronics for wind turbines. IEEE Trans Power Electron. August 2009;24(8):1859–1875. doi:10.1109/TPEL.2009.2017082

[25] Muyeen SM, Takahashi R, Tamura J. Operation and control of HVDC-connected offshore wind farm. IEEE

Trans Sust Energy. Apr 2010;1(1):30–37. doi:10.1109/TSTE.2010.2041561

[26] Mesemanolis A, Mademlis C, Kioskeridis I. Maximum efficiency of a wind energy conversion system with a PM synchronous generator. In: IEEE-MedPower 2010, Power Generation, Transmission, Distribution and Energy Conversion, Proceedings of 7th Mediterranean Conference and Exhibition on; November 2010. p. 1–9.

[27] Blaabjerg F, Iov F, Chen Z, et al. Power electronics and controls for wind turbine systems. In: Energy Conference and Exhibition (EnergyCon), IEEE Conferences; December 2010. p. 333–344.

[28] Abdullah MA, Yatim AHM, Tan CW. A study of maximum power point tracking algorithms for wind energy system. In: IEEE First Conference on Clean Energy and Technology (CET); June 2011. p. 321–326.

[29] Ganesan R, Suresh S, Sivaraju SS. ANFIS based multisector space vector PWM scheme for sensorless BLDC motor drive. In: Microprocessors and Microsystems (Elsevier Science); 2020, p. 1–9.

[30] Oates C, Mondal G. DC circulating current for capacitor voltage balancing in modular multilevel matrix converter. In: Conf. Rec. of European Conference on Power Electronics and Applications (EPE- 2011); 2011, p. 1–7.